ACS OMEGA

Article

Cite This: ACS Omega 2018, 3, 9675−9688

http://pubs.acs.org/journal/acsodf

Cubical-Shaped Rods of Pectin−Hydroxyapatite Composite for Adsorption Studies of Fluoride by Statistical Method and Adsorption Experiments

Sapna Raghav,[†] Sapna,[†] and Dinesh Kumar*[,†,‡]

[†]Department of Chemistry, Banasthali Vidyapith, Banasthali 304022, Rajasthan, India

[‡]School of Chemical Sciences, Central University of Gujarat, Gandhinagar 382030, India

Supporting Information

ABSTRACT: This research details the synthesis and application of a novel pectin−hydroxyapatite (PHAp) composite for fluoride (F^-) adsorption from aqueous solutions. To determine the efficiency of the adsorption process parameters, i.e., adsorbent dose (0.1−0.4 g), initial fluoride concentration (10−30 mg/L), and temperature (298−313 K), the Box−Behnken design with three levels and three factors have been utilized. The quadratic model was established on 27 batch runs by regression analysis of the experimental data of these runs. The efficacy of adsorption was observed using the Langmuir and Freundlich models. The adsorption rate was found at 3.17 mg $g^{-1}min^{-1}$, and adsorption kinetics followed pseudo-second order (PSO) for PHAp. The significant novelty of this work is the synthesis of unique cubical-shaped rods biopolymer composite from hydroxyapatite. Additionally, this composite showed high adsorption capacity for F^- compared to other hydroxyapatite adsorbents, and the improved adsorption capacity is attributed to its unique shape which provides a larger surface area. It can be reused for up to six cycles, which makes this method environment-friendly. The economic viability of the synthesized PHAp composite, in comparison to other adsorbents, is evident from the cost−benefit analysis.

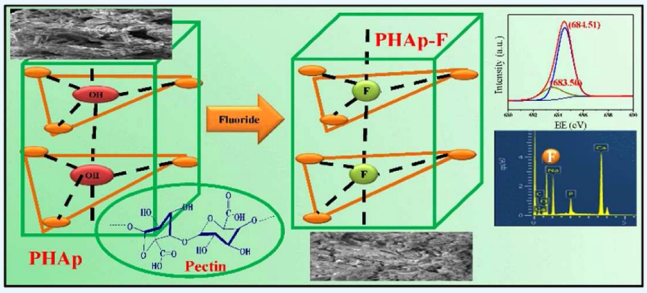

1. INTRODUCTION

The fluoride (F^-), released from industrial effluents, contaminates groundwater. This is of great concern as a high intake of F^- is detrimental to human health, causing skeletal and dental fluorosis and neurological damages. Periodic weathering of rocks and minerals add F^- into groundwater. The waste released from the glass and ceramic industries, electroplating, coal-fired power stations, and so on are other sources that increase the F^- level in groundwater. These effluents can increase the F^- level up to 10−1000 mg/L. The excess F^- uptake through drinking water has an adverse effect on the health of several million people, primarily in developing countries. Although F^- at low doses protects teeth from degradation, exposure to higher concentrations of fluoride can cause dental fluorosis. The beneficial dose and harmful levels are comparatively closer; the testified ideal value to avoid tooth decay is 0.5 mg/L, i.e., below the permissible limit of 1.5 mg/L suggested by the WHO. Hydroxyapatite ($Ca_{10}(PO_4)_6(OH)_2$, HAp), the key constituent of bones and teeth, is responsible for both detrimental and therapeutic health effects of fluoride. Due to the F^- uptake nature of HAp, it has been used in water treatment.[1−8]

Therefore, it is necessary to design a highly selective and rapid method for elimination of F^-. The conventional methods of F^- removal are reverse osmosis,[9] nanofiltration,[10] ion exchange,[11,12] and adsorption.[13] Among these methods, adsorption is favorable due to its economic feasibility. Adsorption is suitable for removing contaminants in trace level and has become increasingly popular in water treatment applications owing to its simplicity, cost-effectiveness, efficiency, easy operation, and lower waste generation.

Recently, various low-cost adsorbents (i.e., activated alumina,[14] carbon nanotubes,[15] bone char,[16] fly ash,[17] metal oxide,[13] etc.) have been used for F^- removal. The traditional adsorbents have limited application due to their low adsorption capacity; hence, research is vital to produce new and effective materials for F^- removal. Of late, biosorption technique (an eco-friendly technique) has been predominantly used. Hydroxyapatite (HAp, $Ca_{10}(PO_4)_6(OH)_2$), the main essential mineral of vertebrate skeletal systems, is efficient as an adsorbent for removal of F^-. HAp is a biomineral that is used in water treatment due to its eco-friendly nature, easy availability, low cost, and presence of excess exchangeable hydroxyl groups. However, their brittleness limits the application of HAp. Additionally, due to excess pressure drop during field application, its powder cannot be utilized in

Received: June 13, 2018
Accepted: August 9, 2018
Published: August 21, 2018

DOI: 10.1021/acsomega.8b01330
ACS Omega 2018, 3, 9675−9688

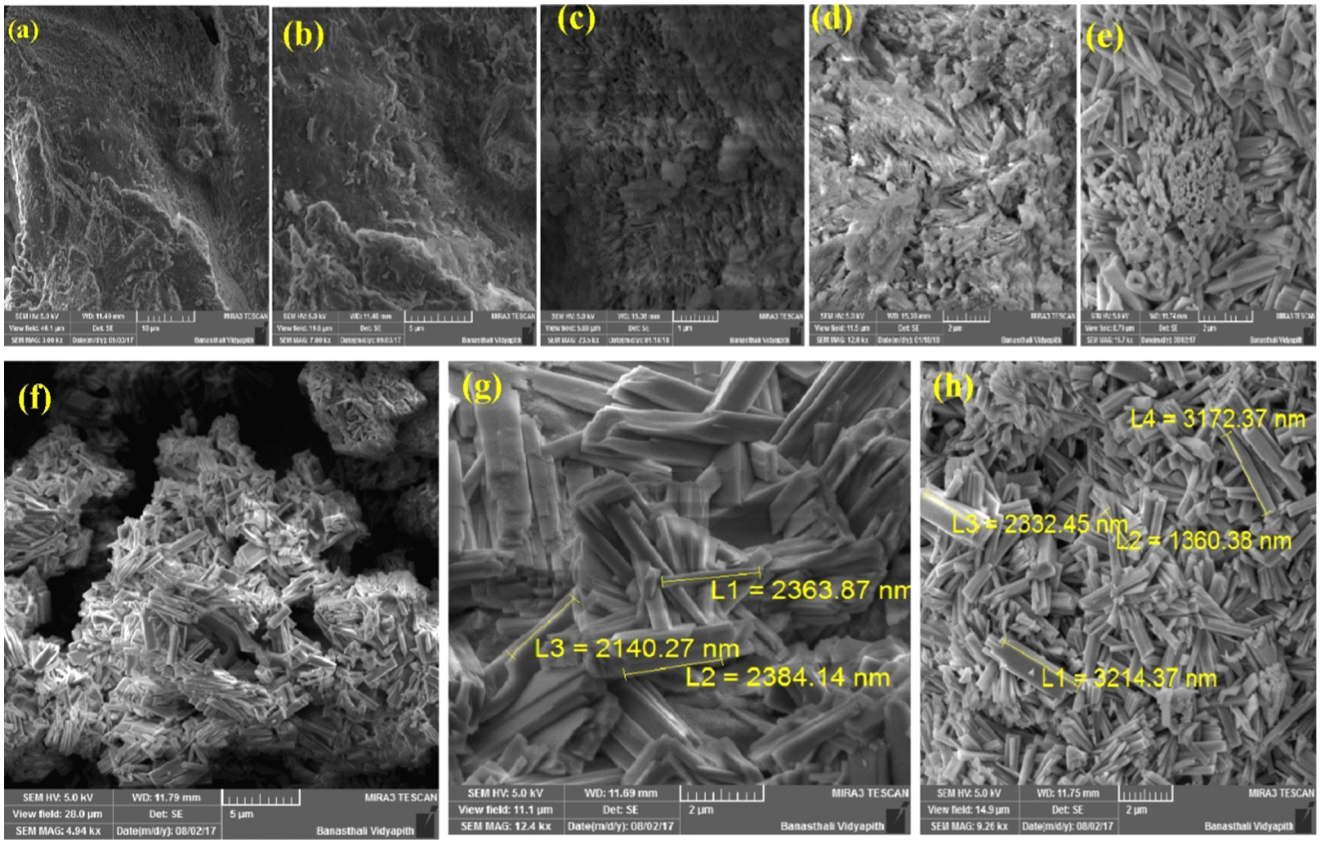

Figure 1. FESEM images of (a, b) pectin, (c, d) PHAp-F, and (e–h) PHAp at different views of cubical rods.

fixed-bed column directly. To overcome these technological issues, polymeric composites have been studied. Biopolymer-supported inorganic composites and their synthesis are in limelight these days due to their exceptional structure and properties.[18−20] Furthermore, the synergistic effect involved in these composites will provide additional mechanical strength to the composite.

Pectin is a type of bio-renewable, nontoxic, inexpensive, and biodegradable natural plant ionic polysaccharides, mainly composed of α-(1→4)-linked D-galacturonic acid.[21,22] These are biocompatible, biofunctional, nontoxic, nonimmunogenic, and biodegradable. Advanced studies mainly focus on biopolymer composites of HAp due to its high surface area and reactivity. In this study, a novel synthesis of pectin–hydroxyapatite (PHAp) composite with the utilization of new biopolymer in F^- adsorption studies is discussed. Additionally, the unique feature of this composite is its shape, which enhances the adsorption sites as well surface area (157 m^2/g), and hence the adsorption capacity (28.47 mg/g). Although to the best of the author's knowledge, there is no work reported on differently shaped adsorbents for F^- removal studies by using biopolymer composite adsorbent, Prabhu et al. reported dendrimer-like hyperbranched chitosan composite for F^- removal having an adsorption capacity of 17.44 mg/g.[23]

The collection of statistical and mathematical techniques, which is called response surface methodology (RSM), was used for empirical model building to overcome the limitations of traditional methods. It is most convenient, particularly in adsorption or removal process,[24] for modeling mechanism parameters. The specific utilization of RSM is to dictate the most advantageous operational conditions for a specific system or to check a region that satisfies the operational specifications.[25,26] The successful synthesis of PHAp adsorbent has been done and it was characterized by Brunauer–Emmett–Teller (BET), field-emission scanning electron microscopy (FESEM), energy-dispersive X-ray analysis (EDAX), X-ray photoelectron spectroscopy (XPS), Fourier transform infrared (FTIR), X-ray diffraction (XRD), and thermogravimetric analysis (TGA) studies. Additionally, the effect of temperature, adsorbent dosage, initial concentration, and other factors on F^- removal by Pec–HAp composite was inspected by using the Box–Behnken design (BBD) in RSM. Langmuir and Freundlich's models were applied to study the adsorption mechanism, and pseudo-first-order (PFO) and pseudo-second-order (PSO) models were utilized to examine the kinetics of the adsorption process. The thermodynamic analysis was used to study the adsorption process feasibility, spontaneity, and nature.

The novelty of this research is the preparation of PHAp composite of unique shape (cubical rod shape), which has a high adsorption capacity due to the availability of six planes for the adsorption compared to other planar adsorbents, which provide only a single planar surface (Figure S1).

2. DISCUSSION OF EXPERIMENTAL OUTCOMES

2.1. Characterization. *2.1.1. FESEM and EDAX Mapping.* Figure 1 shows the FESEM images of pectin (a, b), PHAp-F (c, d), and PHAp (e–h). The FESEM images clearly show the cubical rod shape of PHAp at different angles at 1–5 μm scale. Figure 1e shows the upper morphology of vertically standing rods, Figure 1f (5 μm) shows the agglomerated form of rods, and Figure 1g (5 μm) shows dispersed rod shape, which shows the dissimilar length of rods. After F^- adsorption, the shape of

DOI: 10.1021/acsomega.8b01330
ACS Omega 2018, 3, 9675–9688

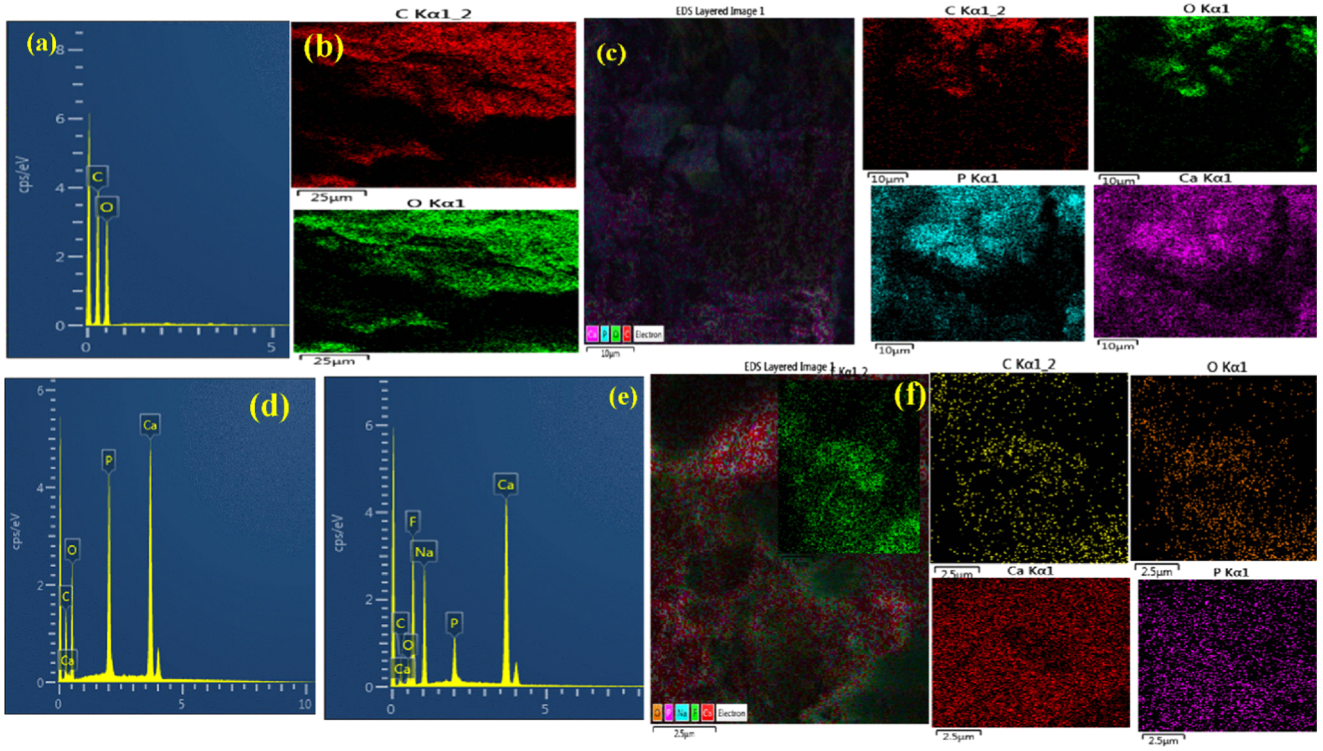

Figure 2. (a, b, d) EDX images of pectin, PHAp, and PHAp-F and (c, e) mapping images of PHAp and PHAp-F.

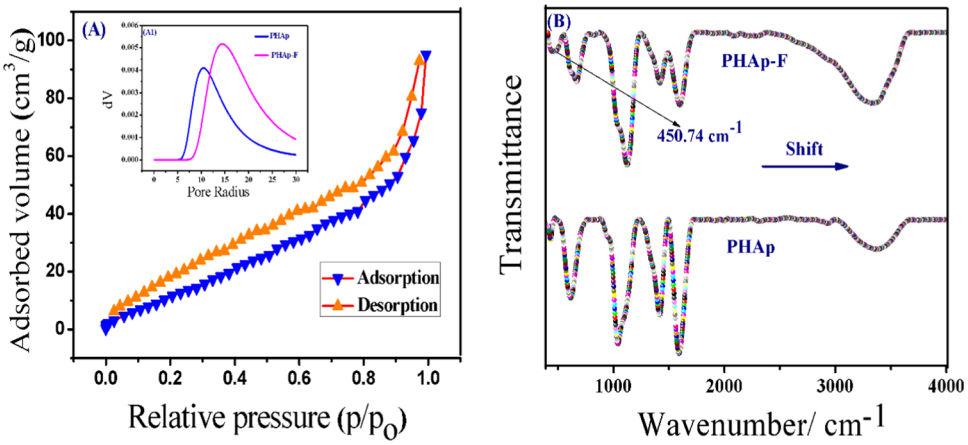

Figure 3. (A) Hysteresis curve, (A1) *D*−*A* pore size distribution, (B) FTIR spectra of PHAp and PHAp-F.

the composite was destroyed, due to the accumulation of spherical shaped F^- on the rods, which is clearly shown in Figure 1c,d. The pectin shows the irregular shape of the polymer. Moreover, Figure 2 shows the EDAX spectrum of synthesized PHAp (Figure 2d), demonstrating the existence of C, O, Ca, and P elements, while in PHAp-F (Figure 2e), one sharp peak of the extra element appears in the EDAX spectrum. The EDAX spectrum of pectin shows only two peaks of C and O (Figure 2a), which shows the purity of the polymer as well as the synthesized compound.

Including the EDAX spectrum of the composite before and after F^- adsorption, EDAX mapping images further supported the elemental composition of pectin, PHAp, and PHAp-F (Figure 2b,c,f, respectively).

2.1.2. BET. Figure 3A shows the N_2 adsorption−desorption isotherms of type IV, and the corresponding pore size distributions are shown in Figure 3A1 of PHAp. The hysteresis loop (type IV) indicated the presence of both micropores and mesopores in the composite. The distributions of the pore volume, pore size, and the surface area before and after F^- adsorption on PHAp are tabulated in Table S1. The BET surface area and the pore volume of PHAp and PHAp-F were found to be 157, 100.0 m^2/g and 0.122, 0.981 cc/g, respectively, which were higher than the values reported in the literature.[27,28]

2.1.3. XPS Analysis. XPS was utilized to identify the various chemical species present on the adsorbent surface before and after the F^- adsorption on PHAp. The high-resolution C 1s spectra (Figure 4A,B) were deconvoluted into four distinct peaks that correspond to the sp^2−C, sp^3−C, C−OH, and C═O bonds at 284.26, 284.50, 285.74, and 288.61 eV.

Oxygen deconvolution spectra (O 1s) for PHAp shows three important contributions at 531.23, 529.37, and 528.83 eV (see Figure 4C,D). These signals can be associated with the oxygen

DOI: 10.1021/acsomega.8b01330
ACS Omega 2018, 3, 9675−9688

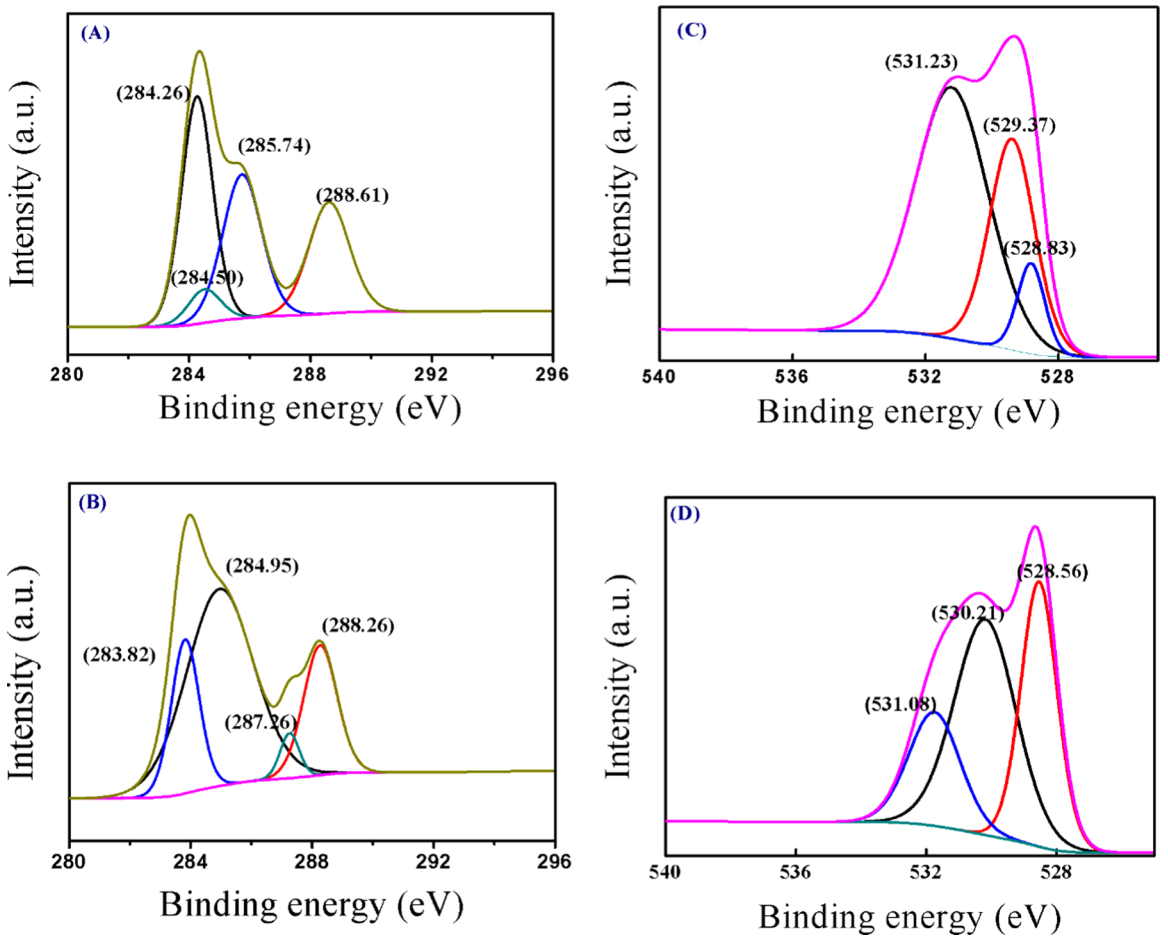

Figure 4. XPS scan of (A, B) carbon and (C, D) oxygen before and after F^- adsorption, respectively.

interaction from chemisorbed water, calcium, and phosphorus in the PHAp composite. The intensities of the three signals are found to change after the interaction of F^- with PHAp owing to surface modification, and these changes were observed at ~528.56, 530.21, and 531.08 eV (Figure 4C,D). The decreased signal intensity was observed at 531.23 and 531.08 eV, which may be due to the interactions between the PHAp and F^- ion. After F^- adsorption, interactions of Ca with F^-, i.e., binding energy of 347.88−351.49 eV, were observed, which also supported the presence of calcium on the surface of the adsorbent. After interaction with F^-, their binding energy shifted to 348.07 and 351.63 eV (see Figure 5A,B). The P 2p XPS image exhibits two peaks at 132.9 eV assigned to P−C and P−N bonds, and the other peak at 133.26 eV corresponding to the P−O bonds of PHAp[29] in Figure 5C,D. The binding energies of all elements before and after F^- adsorption are tabulated in Table S2.

Finally, F 1s XPS images of F^--loaded PHAp are reported in Figure 5E, which contain two signals at 684.51 and 683.50 eV. The peak at 684.51 eV is an evidence of the surface reaction between F^- and Ca^{2+}, which implies the electrostatic interaction mechanism of adsorption. The second peak at 683.50 eV may be due to the replacement of −OH group of PHAp. The above results indicate the important role of hydroxyl groups in F^- adsorption, implying the ion-exchange mechanism of F^- adsorption.

2.1.4. FTIR Spectroscopy. Strong absorption bands appearing at 1024 and 621 cm^{-1} showed the stretching and bending vibrations of PO_4^{3-} of PHAp (Figure 3B). The absorption band at 1024 cm^{-1} was broad and appeared due to the overlap of C−O−C stretching of pectin and PO_4^{3-} stretching of PHAp. The absorption bands occurring at 1613 and 2935 cm^{-1} were attributed to the stretching vibrations of C−O and C−H groups, respectively. There are two broad bands observed between 2500 and 3550 cm^{-1}. The broad band found in the region from 2500 to 3300 cm^{-1} is due to the stretching of O−H bond in the acid group, and another broad band appearing in the region from 3200 to 3550 cm^{-1} is attributed to the stretching of O−H band in alcohol group. The intensity of the broad band, appearing from 2500 to 3500 cm^{-1}, of −OH bond in the acid group was decreased in the F^--adsorbed PHAp composite due to the exchange of the −OH group present in the composite by F^-. The extra peak at 465 cm^{-1} is attributed to the F^- peak.[30,31]

2.1.5. XRD. From Figure 6A, the crystalline peaks of HAp appearing at 2θ (25.92, 32, 33, 35, and 39.81°) were found in the PHAp composite, which showed that no obvious changes were found in the peak structure after the formation of composite and confirmed that the crystal structure of n-HAp was intact in PHAp composite.[32]

2.1.6. TGA. The TGA curve of the PHAp (Huo et al.) exhibits the loss of mass in three steps. The first step, in general, is attributed to a weight loss of about 1.25 mg (10%) in the temperature range of 25−200 °C, which may be due to release of water within this temperature range, while the second degradation step, with 4% weight loss in the

DOI: 10.1021/acsomega.8b01330
ACS Omega 2018, 3, 9675−9688

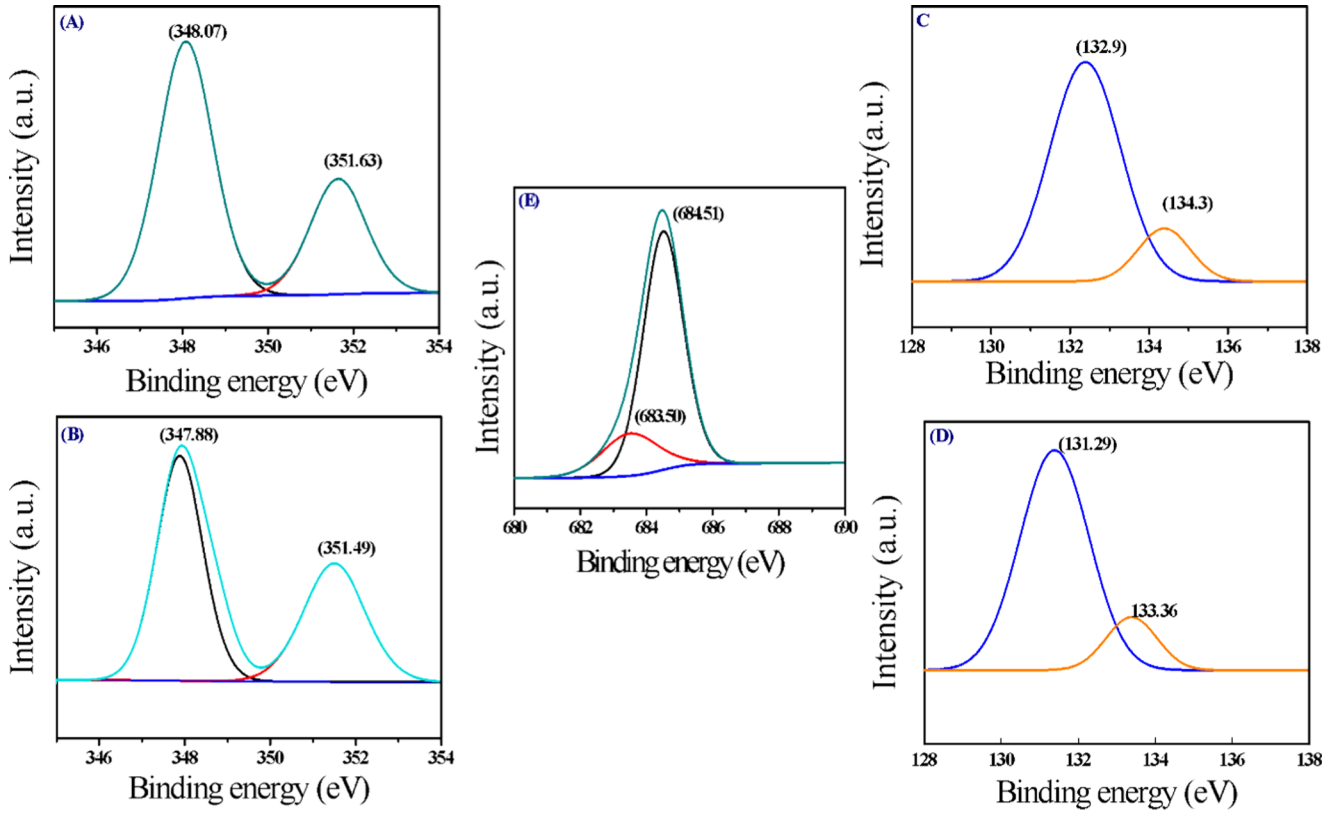

Figure 5. XPS scan of (A, B) calcium and (C, D) phosphorous before and after F^- adsorption, respectively, and (E) F^-.

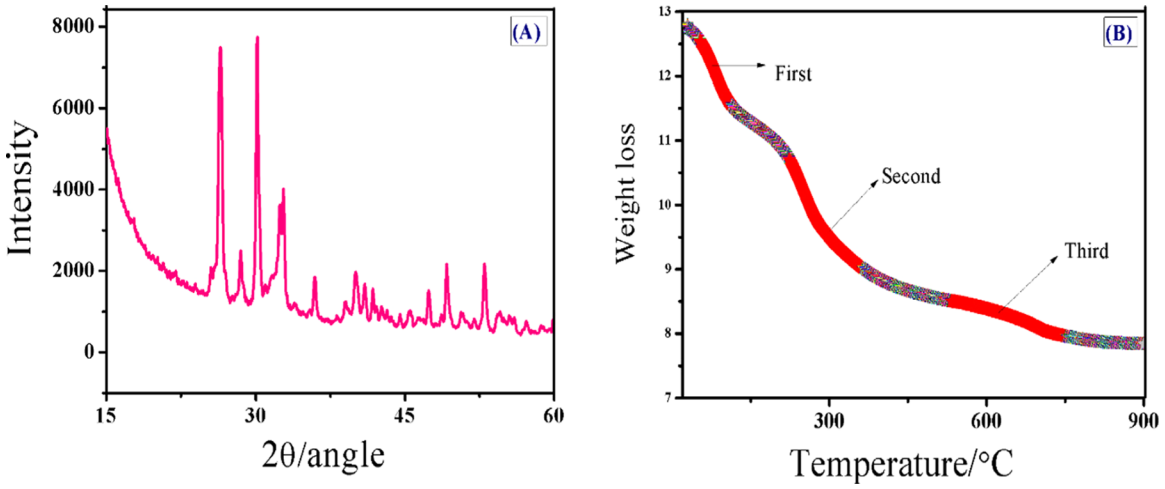

Figure 6. (A) XRD pattern and (B) TGA curve of PHAp.

temperature range of 200−400 °C, was found to be due to the removal of −OH groups. The third degradation step contributed to a weight loss of 1.25 mg (10%) in the temperature range of 400−800 °C assigned by weak endothermic peaks could be related to some phase transformations[33,34] in structures (Figure 6B).

2.2. Development of Regression Model Equation for RSM. The RSM methodology of statics was utilized to construct a relation between the %*A* of F^- and its depending parameters, i.e., three independent variables (adsorbent dose, C_i, and temperature), which directly affect the adsorption. The relation between independent variables and %*A* is in the form of a second-order polynomial equation. The polynomial equation, in the quadratic form, is designed on the analysis of coded or actual factor for %*A* of F^-, and the equation obtained is shown in eq 1

$$\%A = 88.39 + 5.43A + 6.47B - 1.98C - 1.28AA - 2.65BB + 0.88CC - 2.96AB - 0.0008AC + 1.61BC \quad (1)$$

The positive or negative term defines the synergistic or antagonistic effect of the term, respectively. Analysis of variance (ANOVA) results of F^- adsorption by PHAp are tabulated in Table 1. ANOVA was utilized to study the accuracy of the generated model, as well as to examine the fitness of the model and the main and interaction constants of

DOI: 10.1021/acsomega.8b01330
ACS Omega 2018, 3, 9675−9688

Table 1. Response Surface Regression: %*A* vs Temperature, Adsorbent Dose, and Initial F^- Concentration

parameters	coefficient	seq. SS	*F*	*p*
A	5.43	532.68	610.28	0.00
B	6.47	713.54	817.48	0.00
C	−1.98	70.84	81.16	0.00
AA	−1.28	9.92	11.36	0.007
BB	−2.65	42.26	48.41	0.00
CC	0.88	0.09	0.10	0.082
AB	−2.96	105.49	120.86	0.00
AC	−0.0005	0.00	0.00	0.99
BC	1.61	35.16	40.28	0.00
constant	88.39			

the polynomial equation. The *F* value of the designed model was found to be 29.97, with lower probability (<0.0001) indicating that the model was significant.

From the polynomial eq 1, it can be concluded that of the three variables, $B(C_i)$, initial F^- concentration had the major effect on the %*A* of F^-, due to the maximum *F* value. Variable *A*, i.e., adsorbent dose, is followed by *B*, again according to the *F* value. $p > 0.05$ is not significant for the designed model. In adsorption studies, all linear terms are significant, i.e., *A*, *B*, *C* (adsorbent dose, C_i, temperature), and quadratic terms (*AA*, *BB*) are significant, whereas only *AB* and *BC* are significant for the interaction terms. Other variables such as *CC* and *AC* do not have a significant effect on the F^- adsorption due to the *p*-value which is >0.05.[31,35−37]

2.2.1. Effects of Variables on F^- Adsorption. To understand the interaction between independent variables and their results, three-dimensional response surface plots (RSP) and two-dimensional counter plots of the designed model were constructed by utilizing the MINITAB 16.0 software (Figures 7−9 and S2). The RSP envision the interaction effects of each

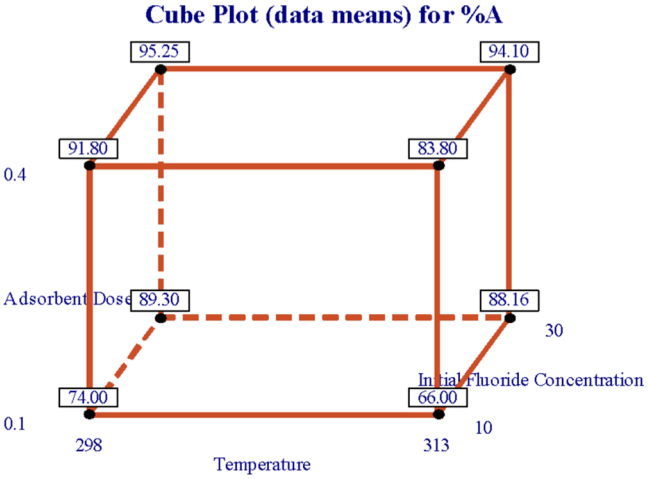

Figure 7. Cube plot for %*A*.

independent variable, which influence the %*A* of F^-. The shape of the contour plot shows the nature and extent of the interactions effects among the experimental factors on the %*A*.[38] In each plot, the interacting variables were changed within the experimental assortments, while the third variable was constant or at the highest level.

2.2.2. Effect of Adsorbent Dose, C_i, and Temperature. Figures 7−9 show the collective effect of two factors alternatively, i.e., adsorbent dose and C_i, adsorbent dose and temperature, C_i and temperature, etc. The cube plot in Figure 7 shows all three factors together in the form of their %*A* values with all three levels. Adsorbent dose and C_i both show a positive effect, and temperature shows a negative effect on %*A* of F^-, i.e., with an increase in adsorbent dose and C_i, %*A* increases, while with an increase in temperature, %*A* decreases (Figure 9). In case of adsorbent dose and C_i, %*A* increases because at a higher adsorbent dose, there is a number of active sites and with high C_i, there is a number of F^- ions for adsorption. Hence, with the increase in the adsorbent dose (0.4 g) and C_i, the adsorption will be comparatively higher.[39]

In case of adsorbent dose and temperature (Figure 9), it was concluded that F^- adsorption decreases with increase in temperature and increases with increasing absorbent dose. This observation might be due to the fact that at constant C_i, an increase in adsorbent dose increases both surface area and the availability of active sites on PHAp molecules, which leads to enhanced F^- adsorption. In case of temperature and C_i (Figure S2) on the F^- adsorption onto PHAp at adsorbent dose 0.4 g, F^- adsorption increases with increase in C_i because when the C_i increases, the active sites of the adsorbent will be surrounded by a greater number of F^-. The increase in %*A* is very little with increasing temperature. This may be due to the increased number of binding sites with increasing temperature and hence the augmenting adsorption.

2.3. Adsorption Property. *2.3.1. Effect of Initial pH.* In the adsorption process, pH of the solution plays a significant role: it controls the adsorption of F^- on the PHAp at the adsorbent interface. The pH effect was studied at a C_i of 10 mg/L, and pH ranges from 3 to 11 (Figure 10A). Percent adsorption of F^- increases up to 7.0 (9.5 mg/g) and then decreases from 7 to 11 (8.6 mg/L). This change can be explained by the surface charge of PHAp in both alkaline and acidic mediums. It is well known that in acidic medium, i.e., pH < 7, the adsorbent surface is highly protonated and hence maximum F^- is adsorbed in acidic medium, due to opposite charges of adsorbent and F^-, and the opposite is true for alkaline media[40] (pH > 7).

2.3.2. Effect of Co-ions. The effect of co-ions on q_e of PHAp was analyzed by comparing the fluoride q_e with co-ions and without co-ions, for which initially fixed concentration of fluoride solution was analyzed by fluoride meter and then a similar concentration of co-anion, such as SO_4^{2-}, with the fluoride solution was analyzed. Similarly, other co-anions, viz., Cl, NO_3^-, and HCO_3^- were also analyzed with fluoride solution. Analysis (Figure 10B) results shows the decrease in q_e with co-anions because they compete with each other for the active sites on the adsorbent surface. The competition of anions for the active sites is closely related to the charge/radius (Z/r) ratio, ionic radii, and their concentration. The order of Z/r values is as follows: Cl^- (1/0.181 nm) < NO_3^- (1/0.179 nm) < SO_4^{2-} (2/0.230 nm). Ions with high Z/r values have high affinity with adsorbent and hence the multivalent anions with smaller radii have greater affinity than the monovalent anions. Therefore, SO_4^{2-} competes more and reduces q_e greater than the monovalent (NO_3^- and Cl^-) anions. But this trend is not applicable in the case of OH^- and HCO_3^-, and the effect of these two anions may be regulated by the ionic radii. Due to almost similar ionic radii of HCO_3^- (0.157 nm) ion with F^- (0.133 nm) ion, it competes with fluoride strongly and decreases q_e more than other ions. The decrease in q_e is also due to the increase in solution pH in the presence of

DOI: 10.1021/acsomega.8b01330
ACS Omega 2018, 3, 9675−9688

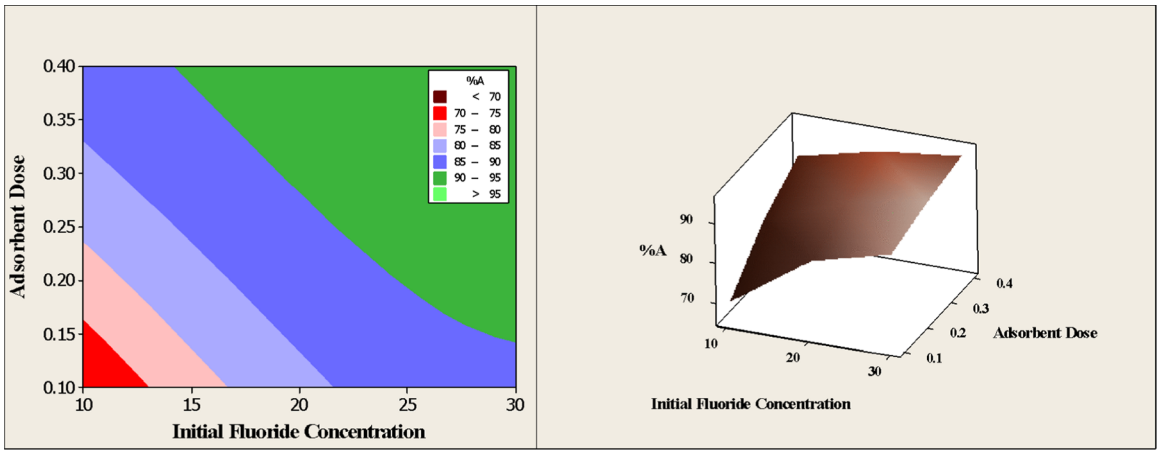

Figure 8. Contour and surface plots of interaction between C_i and adsorbent dose.

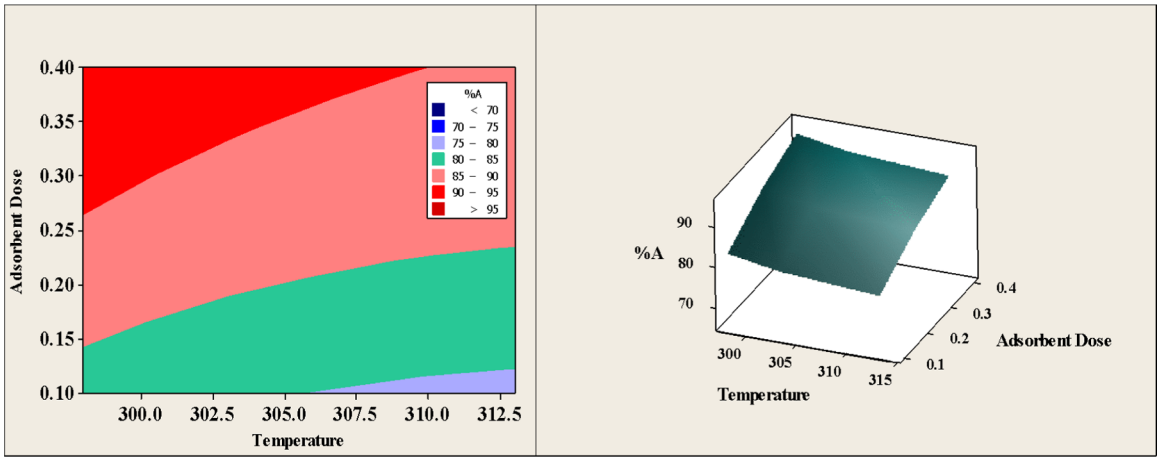

Figure 9. Contour and surface plots of interaction between adsorbent dose and temperature.

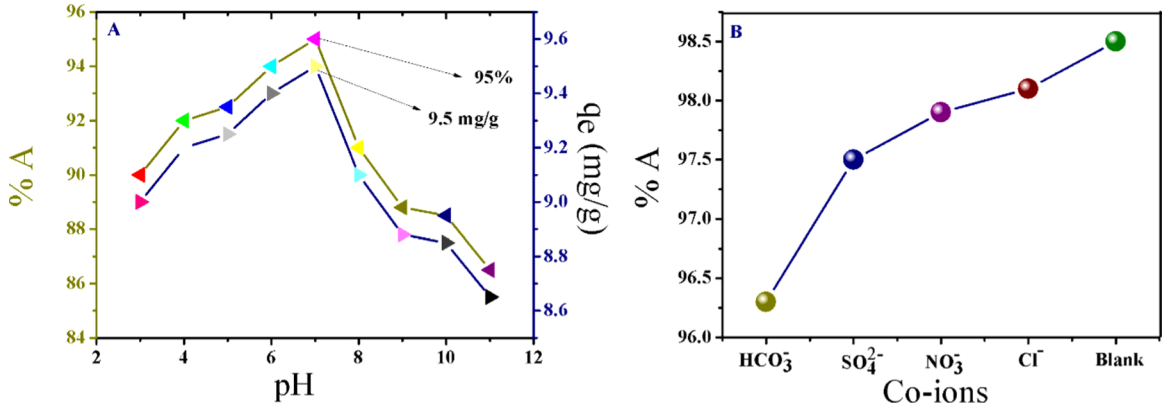

Figure 10. (A) Effect of pH and (B) co-ions on F^- adsorption.

HCO_3^-.[41−43] The F^- ion fits better into the crystal structure of apatite due to its smaller ionic radii and it can substitute OH^- in HAp and form the more thermodynamically stable fluorapatite ($Ca_{10}(PO_4)_6F_2$). Therefore, the order of %*A* in the presence of coexisting anions is $Cl^- < NO_3^- < SO_4^{2-} < HCO_3^-$. However, q_e of the PHAp adsorbent is much lower in the presence of HCO_3^- ion, i.e., 96.25%, owing to its greater interaction with an adsorbent, which reduces the active sites for F^- adsorption.

2.4. Adsorption Isotherms. To compute q_e of PHAp for F^- adsorption, Langmuir (Figure 11A)[44] and Freundlich (Figure 11B)[45] isotherms have been studied at four different temperatures (298, 303, 308, and 313 K) Table 2. Langmuir isotherm model illustrated the monolayer adsorption on the homogeneous surface. Langmuir parameters are related to the maximum adsorption capacity (q_m), and binding affinity of adsorbate to the adsorbent (K_L). A high q_e of 28.57 mg/g at 298 K accounts for good adsorption behavior of PHAp compared to other biopolymer composites of HAp for F^-, as

DOI: 10.1021/acsomega.8b01330
ACS Omega 2018, 3, 9675−9688

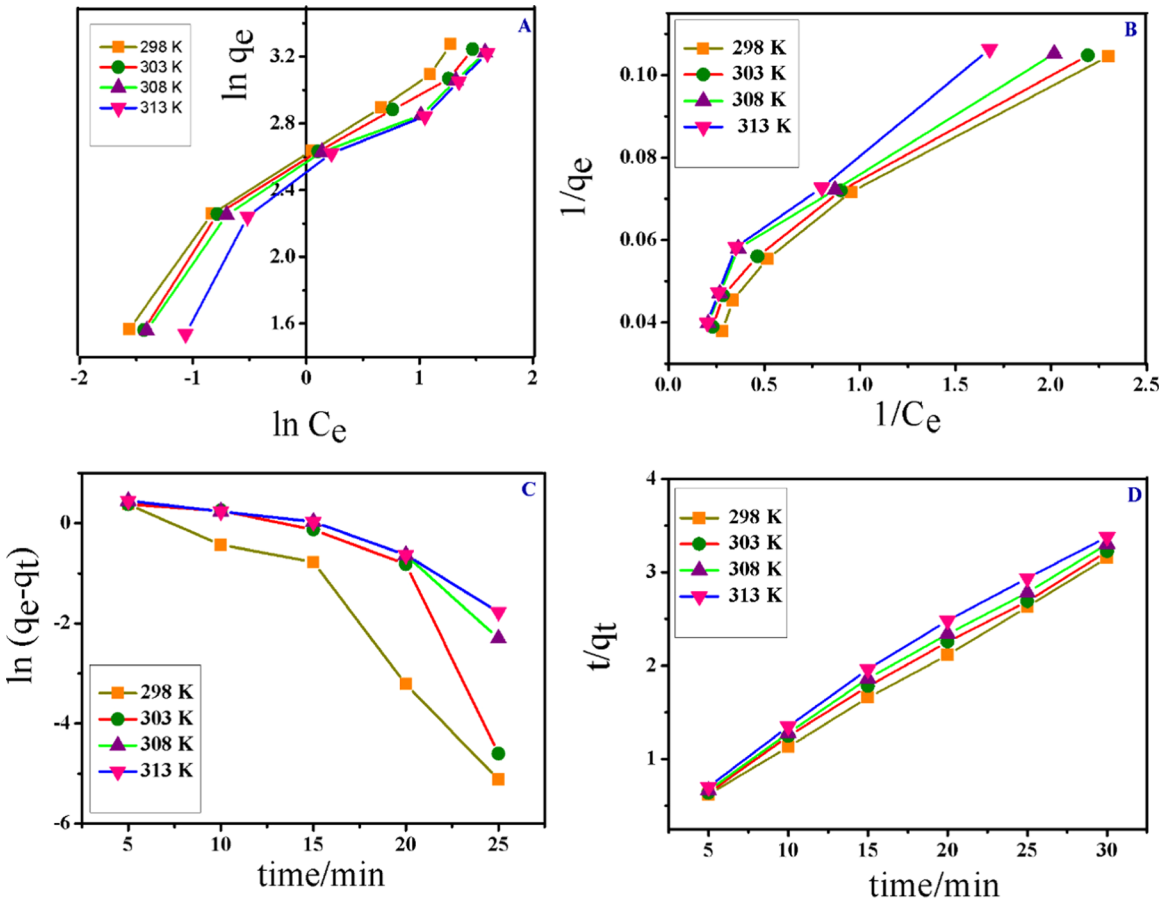

Figure 11. (A) Freundlich, (B) Langmuir isotherms, (C) PFO, and (D) PSO models at four different temperatures 298, 303, 308, and 313 K.

Table 2. Adsorption Parameters of Langmuir and Freundlich Isotherms

	Langmuir					Freundlich			
	$1/q_e = 1/(q_m \times K_L \times C_e) + 1/q_m$					$\ln q_e = \ln K_F + 1/n(\ln C_e)$			
temp (K)	q_m	$1/q_m$	K_L	R_L	R^2 (L)	R^2 (F)	$1/n$	N	K_F
298	28.57	0.035	0.86	0.103	0.95	0.96	0.55	1.81	94.63
303	26.31	0.038	0.82	0.107	0.95	0.94	0.52	1.92	88.23
308	25.64	0.039	0.84	0.105	0.94	0.94	0.50	2	83.93
313	25	0.040	1.03	0.08	0.96	0.92	0.48	2.08	76.70

shown in Table 3. A dimensionless separation factor R_L describes the feasibility of the adsorption. The value of R_L < 1 (Table 2) signifies the effectual interaction between PHAp and F^-.

The Freundlich isotherm illustrates the multilayer adsorption of heterogeneous systems and assumes that different sites have several adsorption energies involved. K_F and $1/n$ represent the q_e and intensity of the adsorbent, respectively, in Table 2. It was found that the data fitted with the Langmuir isotherm model, with the highest R^2 value of 0.96.

Table 3. Comparison of q_m of PHAp with Other Adsorbents

s. no	adsorbents	q_m
1.	NaP−HAp nanocomposite[46]	12.69
2.	cellulose@HAp[43]	4.20
3.	cetyltrimethylammonium bromide-coated hydroxyapatite powder[47]	9.39
4	nanohydroxyapatite/chitosan composite[32]	1.56
5	alginate-encapsulated nanohydroxyapatite[30]	3.87
6.	HAp[31]	3.12
7.	PHAp (present study)	28.57

2.5. Adsorption Kinetics. The effect of contact time is a significant factor for the adsorption studies, i.e., kinetic studies. Figure S3 shows the effect of a change in time on F^- adsorption process. It was experientially found that with increase in time, the F^- adsorption increases gradually and reaches up to an equilibrium position after 30 min. Consequently, the contact time for F^- adsorption process was considered as 30 min. To understand the kinetics of the adsorption process, PFO and PSO kinetic models were utilized to correlate the solid−liquid adsorption. Figure 11C,D shows the kinetics of the adsorption process, and the PSO model is the best fit according to the R^2 analysis. These results predicted that the adsorption mechanism of PSO was predominant and that the physisorption process[48,49] controlled the adsorption because k_2 value decreases with increase in temperature, as shown in Table 4.

DOI: 10.1021/acsomega.8b01330
ACS Omega 2018, 3, 9675−9688

Table 4. Kinetic Parameters of PFO and PSO Models Including Regression Coefficients

	PFO			PSO			
	$\ln(q_e - q_t) = \ln q_e - k_1 \times t$			$t/q_t = 1/(k_2 \times q_e^2) + t/q_e$			
temperature (K)	k_1	q_e	R^2	k_2	$\ln k_2$	q_e	R^2
298	0.27	9.97	0.89	0.081	2.5	10	0.99
303	0.22	10.17	0.70	0.051	2.9	9.9	0.99
308	0.12	4.34	0.75	0.048	3.03	9.7	0.99
313	0.10	3.49	0.85	0.041	3.17	9.4	0.99

The activation energy (E_a), defined as the minimum amount of K.E. required for the adsorption to occur, gives an assessed energy barrier that the adsorbate must have to overcome for adsorption to occur. The E_a can be calculated by fitting the kinetic constant of the PSO model by Arrhenius equation at different temperatures[50] (eq 2).

$$\ln k_2 = -E_a/RT + \ln A_o \quad (2)$$

The E_a value was found to be 32.6 kJ/mol (Figure 12B), the value of E_a decides the type of adsorption, and the result of E_a suggesting the adsorption of F^- is related to particle diffusion controlled in this case.[51]

2.6. Thermodynamic Study. The adsorption process was much influenced by temperature. To examine the spontaneity, feasibility, and nature of the adsorption process, the thermodynamic data plays an important role, which can be obtained from eqs 3 to 5.

$$K_C = C_e/q_e \quad (3)$$

$$\ln K_C = \Delta S/R - \Delta H/RT \quad (4)$$

$$\Delta G = -RT \ln K_C \quad (5)$$

As shown in Figure 12, the values of ΔH and ΔS have obtained parameters of the curve $\ln K_C$ versus $1/T$ (Figure 12C), i.e., from the slope and intercept, respectively. From Table S3, the positive value of ΔH and the negative value of ΔG confirmed the endothermic nature of the adsorption process and the feasibility and spontaneous nature of adsorption, respectively. The positive value of ΔS showed an increase in randomness during the adsorption of F^- at the solid−solution interface.[52]

A new concept of sticking probability (S^*) was explained using modified Arrhenius eqs 6 and 7. S^* is related to the surface coverage (θ). This is a measure of the potential of an adsorbent to hold the adsorbate on its surface.[53]

$$\theta = (1 - C_e/C_o) \quad (6)$$

$$\ln(1-\theta) = \ln S^* + E_a/RT \quad (7)$$

Figure 12D shows the graph of surface coverage and $1/T$, and the intercept and slope of the graph give $\ln S^*$ and E_a/R, respectively. The value S^* decides the nature of adsorption. The reported value of S^* reveals the physisorption nature of adsorption (Table S4).

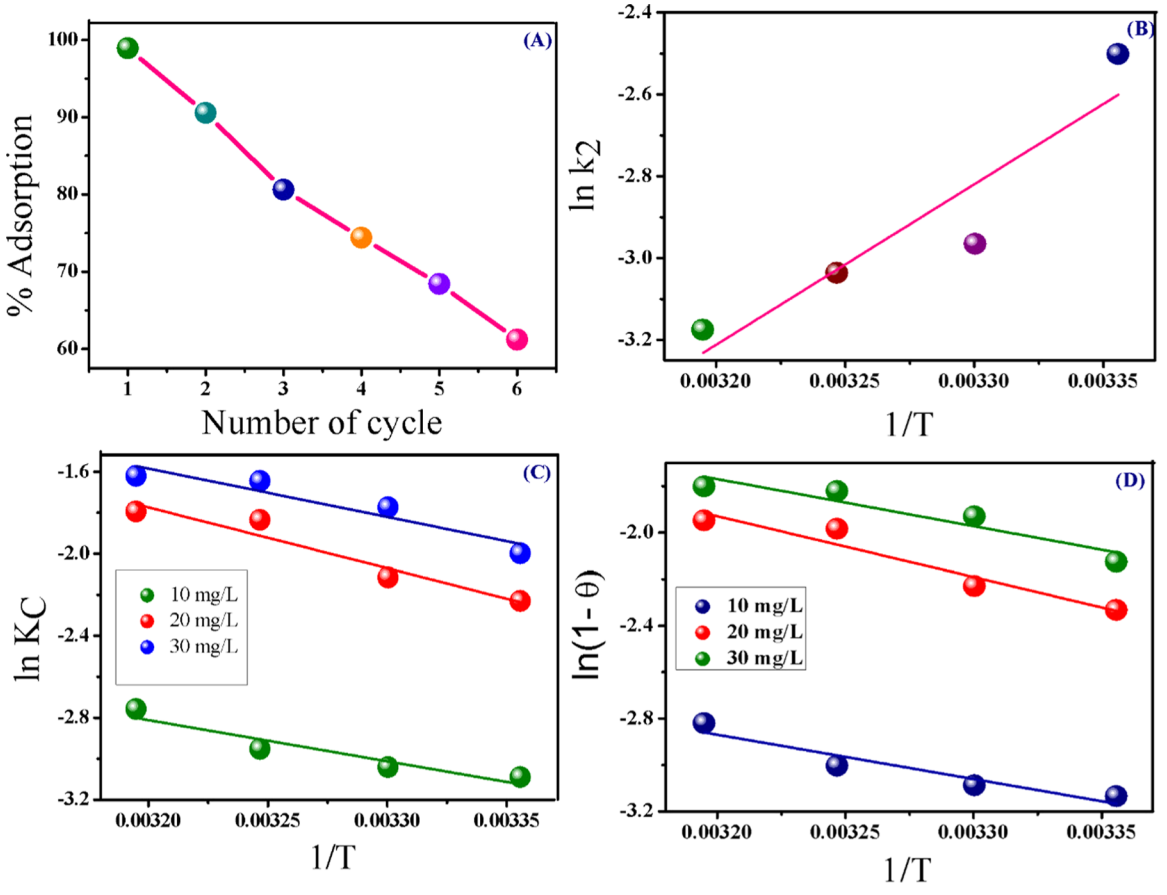

Figure 12. (A) Regeneration cycles, (B) activation energy curve by pseudo-second-order constant, (C) van't Hoff plot, and (D) activation energy by sticking probability.

DOI: 10.1021/acsomega.8b01330
ACS Omega 2018, 3, 9675−9688

2.7. Reusability Studies. The regeneration of PHAp is a significant aspect to utilize adsorbent in practical application (Figure 12A). Table S5 shows the analysis data of repeated %*A* of adsorption−desorption cycles. After every cycle, the filtered adsorbent was washed with 0.01 M HCl/NaOH and then used for the next cycle. This repeated process was done for six cycles, and after six cycles, the %*A* was observed to be decreasing, probably due to the replacement of −OH group by F^- ions. Nevertheless, the regeneration efficacy of the PHAp could be improved by treating the used adsorbent with NaOH/HCl.

2.8. Cost−Benefit Analysis. The cost−benefit analysis for the adsorbent is an important factor for its economic viability. The developed PHAp composite was synthesized by utilizing AR-grade chemicals. The cost−benefit analysis confirmed that the F^- removal cost by PHAp is reasonably good compared to other traditional adsorbents. The cost of PHAp is higher than some traditional adsorbents,[54−58] as shown in Table 5;

Table 5. Comparative Cost of Traditional Adsorbent and PAF

adsorbent	q_m (mg/g)	cost of adsorbent (U.S. $/kg)
activated carbon	2.25	21.1
activated alumina	16.3	12.1
bone char	4.5	1.6
hydrous ferric oxide	13.2	10.42
PHAp	28.57	25.79

however, PHAp had a high adsorption capacity of 28.57 mg/g, which even remained higher (60%) after six successive adsorption cycles. Hence, the synthesized PHAp composite shows good F^- removal efficacy in water.

2.9. Adsorption Mechanism of F^- on PHAp. Thermodynamic studies, spectroscopic investigation, adsorption studies, and kinetic studies all illustrate that the mechanism of adsorption of F^- on PHAp is mainly due to ion exchange, electrostatic interaction, and also by physio-type adsorption (Figure 13). From the XPS and FTIR investigations, the adsorbent has replaceable OH group, which participates in the ion-exchange mechanism. This is also proved by pH studies. At lower pH, the adsorbent surface acquires a positive charge, and hence it electrostatically interacts with negatively charged F^-,

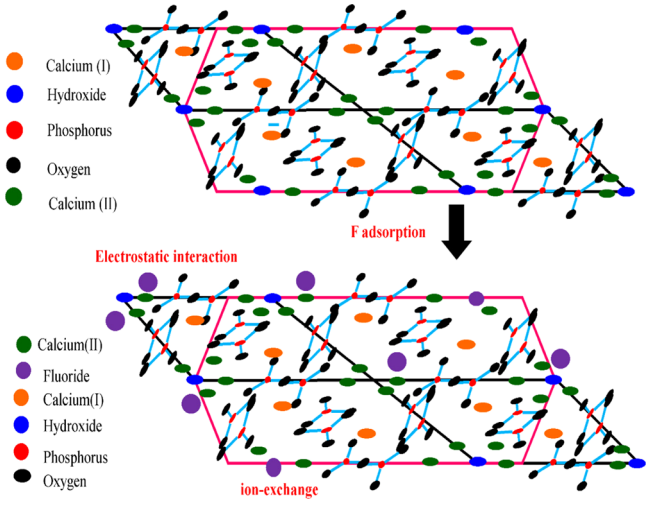

Figure 13. Expected mechanism of F^- adsorption.

while at high pH, the opposite phenomenon works, i.e., adsorbent acquires a negative charge. Additionally, the Ca^{2+} ions present in PHAp interact with F^- ions by electrostatic attraction.

3. CONCLUSIONS

In this work, PHAp composite, an effective adsorbent for F^- adsorption, was synthesized by a simple precipitation method, which produces a cubical-shaped rod-type structure. The PHAp composite was established by several characterizing techniques: BET, FESEM, EDAX, XPS, FTIR, XRD, and TGA. The RSM was combined by BBD to regulate the effect of three factors, i.e., adsorbent dosage, C_i, and temperature, on F^- adsorption. The adsorption process follows PSO kinetics and follows Langmuir type of adsorption, i.e., monolayer adsorption. The q_m for the PHAp adsorption process was found to be 28.57 mg/g. Thermodynamically, the process was feasible, spontaneous, and endothermic in nature, as revealed by the thermodynamic parameters, i.e., ΔG, ΔS, and ΔH. The overall study indicated that PHAp composite can be used as an efficient adsorbent for F^- removal from drinking water and other water sources.

4. EXPERIMENTAL SECTION

4.1. Materials. Chemical reagents predominantly involved pectin, $Ca(NO)_3{\cdot}4H_2O$, NH_3, NaOH, HCl, $NaNO_3$, $NaNO_3$,

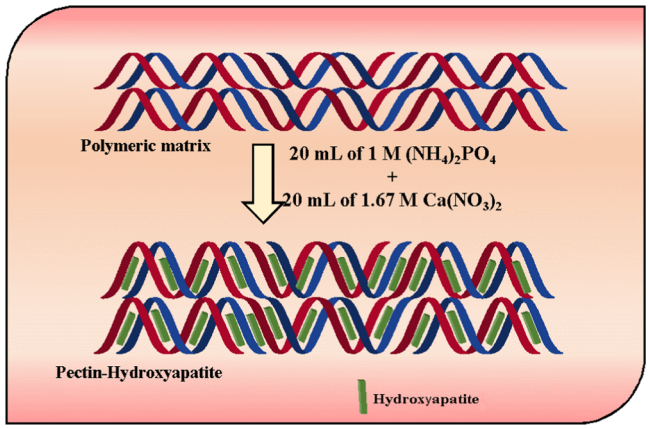

Figure 14. Expected arrangement of HAp in pectin polymer.

Table 6. Independent Variables and Their Coded Levels to RSM Design

independent variables/factors	units	−1	0	+1
adsorbent dose (*A*)	g	0.1	0.25	0.4
C_i (*B*)	mg/L	10	20	30
temperature (*C*)	K	298	308	313

NaCl, NaF, $(NH_4)_2PO_4$, etc. All chemicals were of analytical grade and utilized without further purification. Deionized (DI) water was utilized during the preparation of adsorbent and adsorption experiments.

4.2. Preparation of PHAp Adsorbent. Pectin (2 g) was dissolved in 100 mL of DI water at room temperature, and the mixture was continuously stirred to obtain a homogeneous solution. Then, 20 mL of 1 M $(NH_4)_3PO_4$ solution was added dropwise into the polymer solution within 15 min. The pH of the solution was maintained up to 10 using 25% NH_3 solution. Then, 20 mL of 1.67 M calcium nitrate solution was added to

DOI: 10.1021/acsomega.8b01330
ACS Omega 2018, 3, 9675−9688

Table 7. Batch Runs for RSM Experiment

runs	%A	A	B	C
1.	74	10	0.1	298
2.	85	10	0.25	298
3.	91.8	10	0.4	298
4.	85	20	0.1	298
5.	90.5	20	0.25	298
6.	93.9	20	0.4	298
7.	89.3	30	0.1	298
8.	93	30	0.25	298
9.	95.25	30	0.4	298
10.	69.5	10	0.1	313
11.	80.5	10	0.25	313
12.	87.3	10	0.4	313
13.	83.5	20	0.1	313
14.	89	20	0.25	313
15.	92.4	20	0.4	313
16.	89	30	0.1	313
17.	92.66	30	0.25	313
18.	94.93	30	0.4	313
19.	66	10	0.1	308
20.	77	10	0.25	308
21.	83.8	10	0.4	308
22.	82.25	20	0.1	308
23.	87.75	20	0.25	308
24.	91.15	20	0.4	308
25.	88.16	30	0.1	308
26.	91.83	30	0.25	308
27.	94.1	30	0.4	308

the above solution for 30 min and stirred vigorously for 1 h, after which the solution was left for 24 h at RT. Then, the solution was filtered and washed with DI water to remove some impurities, and the precipitate obtained was PHAp. The precipitate was dried at 100 °C for 6 h and then crushed into a fine powder. The expected arrangement of HAp in pectin polymer is represented in Figure 14. PHAp was also synthesized by varying pH, ripening time, and concentration of calcium ions (Table S6), which are shown in Figure S4. The fine powder obtained was PHAp, which was further utilized for adsorption experiments.

4.3. General Characterization. The N_2 adsorption–desorption isotherms, surface area, and pore size distribution of PHAp before and after F^- adsorption were calculated by using BET analysis. Before the analysis, the samples were kept in vacuum at 300 °C for 4 h for outgassing to remove the volatile gases. To study the surface morphology and element detection, field emission scanning electron microscopy and EDAX analysis were carried out. The binding energy and surface composition of PHAp in both stages were analyzed by XPS analysis. Furthermore, to confirm the functional groups involved in the mechanism and the composition of the adsorbent, FTIR analysis was done using Bruker-FTIR. And to define the crystallography of the structure, XRD analysis was conducted. TGA analysis also was done to know about the thermal behavior of the PHAp using PerkinElmer TGA-4000.

4.4. Statistical Analysis of Adsorption Process. The RSM design was utilized to examine the F^- adsorption on the PHAp. Statistical design for RSM comprises three levels (−1, 0, and +1). The RSM design methods were carried out with three independent variables (adsorbent dose, initial fluoride concentration (C_i), and temperature (Table 6)). Table 7 shows the data obtained from the software after 27 runs per experimental design. Equation 8 demonstrates the effect of variables in terms of linear and quadratic interactions. Then, the statistical calculation was done by using regression coefficients to generate dimensional and contour maps from the regression models. Figure 15 shows the details (step by step) for optimizing F^- adsorption. Minitab software was utilized for the analysis of the experimental data.

The following second-order polynomial equation was utilized to analyze the experimental outcomes of adsorption

$$Y = \beta_0 + \sum_{i-1}^{n} \beta_o X_i + \sum_{i-1}^{n} \beta_{ii} X_i^2 + \sum_{i<j-1}^{n} \beta_{ij} X_i X_j \quad (8)$$

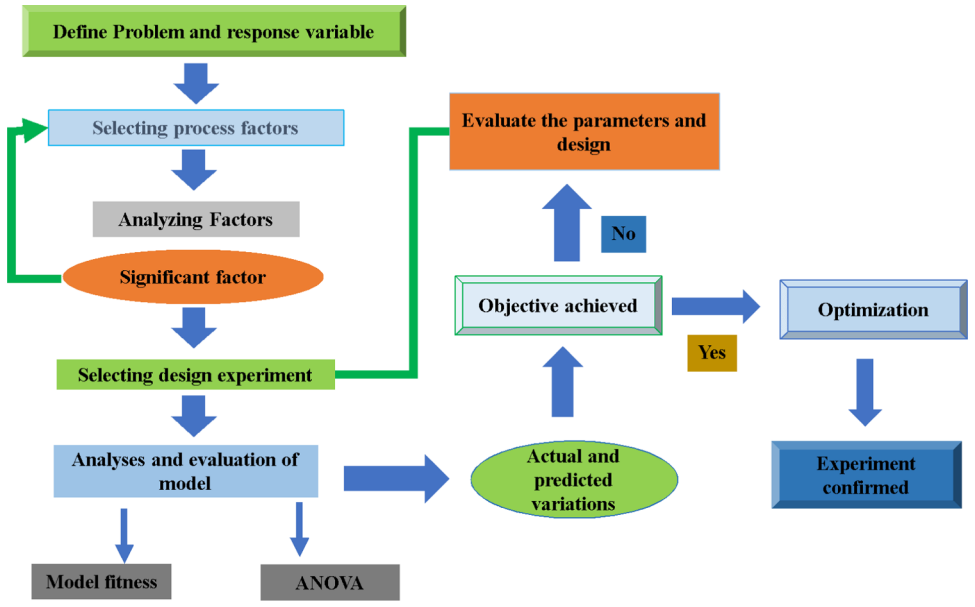

Figure 15. Flowchart for optimization of F^- adsorption.

DOI: 10.1021/acsomega.8b01330
ACS Omega 2018, 3, 9675−9688

where Y is the predicted response (%A) and β_o, β_i, β_{ij}, β_{ii}, and X_i, X_j are the offset term, linear effect, first-order interaction, quadratic effect, and independent variables constants of the model, respectively. ANOVA was applied to study the adsorption behavior, i.e., %A, and independent variable effects (interaction effect), to find the optimum level, and to assess the statistical parameters by means of RSM.

4.5. Adsorption Experiments. All adsorption tests were carried out with C_i in the range of 5−100 mg/L, adsorbent dose of 0.1−0.4 g, contact time of 5−45 min, pH of 3−11, temperature of 298−313 K, assorted ion effect (Cl^-, NO_3^-, SO_4^{2-}, and HCO_3^-), and regeneration studies for F^- adsorption onto PHAp. The pH value of the solution was regulated by using 0.1 mol/L HCl or NaOH. The adsorption kinetics of F^- on the adsorbent was studied at four different temperatures (298, 303, 308, and 313 K) and a particular time interval (5−30 min) with the adsorbent dose of 0.4 g/L, C_i of 10 mg/L, and pH of 7.0. The adsorption isotherm trials were examined by altering the C_i from 10 to 100 mg/L at 298, 303, 308, and 313 K. All other conditions are the same as in kinetic studies. The residual F^- concentration after each adsorption experiment was analyzed by F^- equipped ion meter and calculated using eqs 9 and 10.

$$\%A = (C_i - C_e)100/C_i \quad (9)$$

$$q_e = V(C_i - C_e)/m \quad (10)$$

where %A and q_e are % adsorption and adsorption capacity, respectively.

■ ASSOCIATED CONTENT

Supporting Information

The Supporting Information is available free of charge on the ACS Publications website at DOI: 10.1021/acsomega.8b01330.

BET analysis parameter (Table S1); binding energy of respective elements of PHAp and PHAp-F in XPS analysis (Table S2); thermodynamic parameters of adsorption experiment (Table S3); Arrhenius-type equation parameters with sticking probability (Table S4); recyclability data of PHAp adsorbent using 0.1 M NaOH (Table S5); different synthesis condition of PHAp (Table S6); schematic picture of cubical-shaped rods (Figure S1); contour and surface plots of interaction between initial fluoride concentration and temperature (Figure S2); effect of contact time on adsorption of fluoride by PHAp (Figure S3); FESEM images of PHAp at different conditions (Figure S4) (PDF)

■ AUTHOR INFORMATION

Corresponding Author

*E-mail: dsbchoudhary2002@gmail.com.

ORCID

Dinesh Kumar: 0000-0001-5488-951X

Notes

The authors declare no competing financial interest.

No data sets were generated or analyzed during the current study.

■ ACKNOWLEDGMENTS

The authors gratefully acknowledge support from the Ministry of Science and Technology and Department of Science and Technology, Government of India, under the Scheme of Establishment of Women Technology Park, for providing the necessary financial support to carry out this study vide letter F. No. SEED/WTP/063/2014.

■ REFERENCES

(1) Aoudj, S.; Khelifa, A.; Drouiche, N.; Belkada, R.; Miroud, D. Simultaneous removal of chromium(VI) and Fluoride by electrocoagulation−electroflotation application of a hybrid Fe-Al anode. *Chem. Eng. J.* **2015**, *267*, 153−162.

(2) Rakhunde, R.; Deshpande, L.; Juneja, H. D. Chemical speciation of chromium in water a review. *Crit. Rev. Environ. Sci. Technol.* **2012**, *42*, 776−810.

(3) Wang, Y.; Liu, D. F.; Lu, J. B.; Huang, J. Enhanced adsorption of hexavalent chromium from aqueous solutions on facilely synthesized mesoporous iron−zirconium bimetal oxide. *Colloids Surf., A* **2015**, *481*, 133−142.

(4) Barathi, M. A.; Kumar, S. K.; Rajesh, N. Efficacy of novel Al−Zr impregnated cellulose adsorbent prepared using microwave irradiation for the facile defluoridation of water. *J. Environ. Chem. Eng.* **2013**, *1*, 1325−1335.

(5) Li, L.; Li, Y. X.; Cao, L. X.; Yang, C. F. Enhanced chromium (VI) adsorption using nanosized chitosan fibers tailored by electrospinning. *Carbohydr. Polym.* **2015**, *125*, 206−213.

(6) Kaygusuz, H.; Uzasc, S. S.; Erim, F. B. Removal of fluoride from aqueous solution using aluminum alginate beads. *Clean: Soil, Air, Water* **2015**, *43*, 724−730.

(7) Skwarek, E. Adsorption of Zn on synthetic hydroxyapatite from aqueous solution. *Sep. Sci. Technol.* **2014**, *49*, 1654−1662.

(8) Skwarek, E. Application of Silver Tin Research on Hydroxyapatite. *Advanced Ceramic Materials*; Wiley-Scrivener Publishing: MA, 2016; pp 385−417.

(9) Ndiaye, P. I.; Moulin, P.; Dominguez, L.; Millet, J. C.; Charbit, F. Removal of fluoride from electronic industrial effluent by RO membrane separation. *Desalination* **2005**, *173*, 25−32.

(10) Nasr, A. B.; Charcosset, C.; Amar, R. B.; Walha, K. Defluoridation of water by nanofilteration. *J. Fluorine Chem.* **2013**, *150*, 92−97.

(11) Meenakshi, S.; Viswanathan, N. Identification of selective ion−exchange resin for fluoride sorption. *J. Colloid Interface Sci.* **2007**, *308*, 438−450.

(12) Meenakshi, S.; Viswanathan, N. Identification of selective ion-exchange resin for fluoride sorption. *J. Colloid Interface Sci.* **2007**, *308*, 438−450.

(13) Dhillon, A.; Kumar, D. Development of a nanoporous adsorbent for the removal of health−hazardous fluoride ions from aqueous systems. *J. Mater. Chem. A* **2015**, *3*, 4215−4228.

(14) Ghorai, S.; Pant, K. K. Investigations on the column performance of fluoride adsorption by activated alumina in a fixed-bed. *Chem. Eng. J.* **2004**, *98*, 165−173.

(15) Srivastava, S. Sorption of divalent metal ions from aqueous solution by oxidized carbon nanotubes and nanocages a review. *Adv. Mater. Lett.* **2013**, *4*, 2−8.

(16) Medellin-Castillo, N. A.; Leyva-Ramos, R.; Ocampo-Perez, R.; Garcia de la Cruz, R. F.; Aragon-Pina, A.; Martinez-Rosales, J. M.; Guerrero-Coronado, R. M.; Fuentes-Rubio, L. Adsorption of fluoride from water solution on bone char. *Ind. Eng. Chem. Res.* **2007**, *46*, 9205−9212.

(17) Oguz, E. Equilibrium isotherms and kinetics studies for the sorption of F^- on light weight concrete materials. *Colloids Surf., A* **2007**, *295*, 258−263.

(18) Miretzky, P.; Cirelli, A. F. Fluoride removal from water by chitosan derivatives and composites A review. *J. Fluorine Chem.* **2011**, *132*, 231−240.

DOI: 10.1021/acsomega.8b01330
ACS Omega 2018, 3, 9675−9688

(19) Zhao, X.; Shi, Y.; Cai, Y.; Mou, S. Cetyltrimethylammonium bromide-coated magnetic nanoparticles for the preconcentration of phenolic compounds from environmental water samples. *Environ. Sci. Technol.* **2008**, *42*, 1201−1206.
(20) Zhang, D.; Luo, H.; Zheng, L.; Wang, K.; Li, H.; Wang, Y.; Feng, H. Utilization of waste phosphogypsum to prepare hydroxyapatite nanoparticles and its application towards removal of F^- from aqueous solution. *J. Hazard. Mater.* **2012**, *241*−*242*, 418−426.
(21) Nesic, A. R.; Velickovic, S. J.; Antonovic, D. G. Novel composite films based on amidated pectin for cationic dye adsorption. *Colloids Surf., B* **2014**, *116*, 620−626.
(22) Zhu, J.; Lin, X.; Wua, P.; Luo, X. Pectin/Al_2O_3-ZrO_2 core/shell beads sorbent for fluoride removal from aqueous solution. *RSC Adv.* **2016**, *6*, 27738−27749.
(23) Prabhu, S. M.; Meenakshi, S. A dendrimer like hyperbranched chitosan beads toward F^- adsorption from water. *Int. J. Biol. Macromol.* **2015**, *78*, 280−286.
(24) Sahu, M. K.; Sahu, U. K.; Patel, R. K. Adsorption of safranin-O dye on CO_2 neutralized activated red mud waste: process modelling, analysis and optimization using statistical design. *RSC Adv.* **2015**, *5*, 42294−42304.
(25) Amini, M.; Younesi, H.; Bahramifar, N.; Lorestani, A. A. Z.; Ghorbani, F.; Daneshi, A.; Sharifzadeh, M. Application of response surface methodology for optimization of lead biosorption in an aqueous solution by *Aspergillus niger*. *J. Hazard. Mater.* **2008**, *154*, 694−702.
(26) Massoudinejad, M.; Ghaderpoori, M.; Shahsavani, A.; Amini, M. M. Adsorption of fluoride over a metal organic framework Uio-66 functionalized with amine groups and optimization with response surface methodology. *J. Mol. Liq.* **2016**, *221*, 279−286.
(27) Cai, J.; Zhao, X.; Zhang, Y.; Zhang, Q.; Pan, B. Enhanced fluoride removal by La-doped Li/Al layered double hydroxides. *J. Colloid Interface Sci.* **2018**, *509*, 353−359.
(28) Dhillon, A.; Sapna; Kumar, D. Dual adsorption behavior of F^- from drinking water on Ca-Zn $(OH)_2CO_3$ adsorbent. *Surf. Interfaces* **2017**, *6*, 154−161.
(29) Cai, H.; Chen, G.; Peng, C.; Xu, L.; Zhu, X.; Zhang, Z.; Dong, Y.; Shang, G.; Ke, F.; Gao, H.; Wan, X. Enhanced removal of fluoride by tea waste supported hydrous Aluminium oxide nanoparticles: anionic polyacrylamide mediated aluminum assembly and adsorption mechanism. *RSC Adv.* **2015**, *5*, 29266−29275.
(30) Pandi, K.; Viswanathan, N. Synthesis of alginate bioencapsulated nano-hydroxyapatite composite for selective fluoride sorption. *Carbohydr. Polym.* **2014**, *112*, 662−667.
(31) Mourabet, M.; El Rhilassi, A.; El Boujaady, H.; Bennani-Ziatni, M.; El Hamri, R.; Taitai, A. Removal of fluoride from aqueous solution by adsorption on hydroxyapatite (HAp) using response surface methodology. *J. Saudi Chem. Soc.* **2015**, *19*, 603−615.
(32) Sundaram, C. S.; Viswanathan, N.; Meenakshi, S. Uptake of fluoride by nanohydroxyapatite/ chitosan, a bioinorganic composite. *Bioresour. Technol.* **2008**, *99*, 8226−8230.
(33) Cruciani, G. Zeolites upon heating: Factors governing their thermal stability and structural changes. *J. Phys. Chem. Solids* **2006**, *67*, 1973−1994.
(34) Huo, Z.; Xu, X.; Lu, Z.; Song, J.; He, M.; Li, Z.; Wang, Q.; Yan, L. Synthesis of zeolite NaP with controllable morphologies. *Microporous Mesoporous Mater.* **2012**, *158*, 137−140.
(35) Das, B.; Mondal, N. K.; Roy, P.; Chattoraj, S. Application of response surface methodology for hexavalent chromium adsorption onto alluvial soil of Indian origin. *Int. J. Environ. Pollut. Solutions* **2013**, *2*, 72−87.
(36) Su, S. N.; Nie, H. L.; Zhu, L. M.; Chen, T. X. Optimization of adsorption conditions of papain on dye affinity membrane using response surface methodology. *Bioresour. Technol.* **2009**, *100*, 2336−2340.
(37) Fan, J.; Yi, C.; Lan, X.; Yang, B. Optimization of synthetic strategy of 4′4″(5″)-di-tert-butyldibenzo-18-crown-6 using response surface methodology. *Org. Process Res. Dev.* **2013**, *17*, 368−374.
(38) Massoudinejad, M.; Ghaderpoori, M.; Shahsavani, A.; Amini, M. M. Adsorption of fluoride over a metal organic framework Uio-66 functionalized with amine groups and optimization with response surface methodology. *J. Mol. Liq.* **2016**, *221*, 279−286.
(39) Han, R.; Zhang, J.; Han, P.; Wang, Y.; Zhao, Z.; Tang, M. Study of equilibrium, kinetic and thermodynamic parameters about methylene blue adsorption onto natural zeolite. *Chem. Eng. J.* **2009**, *145*, 496−504.
(40) Xu, C.; Li, J.; He, F.; Cui, Y.; Huang, C.; Jin, H.; Hou, S. Al_2O_3-Fe_3O_4-expanded graphite nano-sandwich structure for F^- removal from aqueous solution. *RSC Adv.* **2016**, *6*, 97376−97384.
(41) Aoba, T. The effect of fluoride on apatite structure and growth. *Crit. Rev. Oral Biol. Med.* **1997**, *8*, 136−153.
(42) Sternitzke, V.; Kaegi, R.; Audinot, J. N.; Lewin, E.; Hering, J. G.; Johnson, C. A. Uptake of F^- from aqueous solution on nano-sized hydroxyapatite: examination of a fluoridated surface layer. *Environ. Sci. Technol.* **2012**, *46*, 802−809.
(43) Yu, X.; Tong, S.; Ge, M.; Zuo, J. Removal of F^- from drinking water by cellulose@hydroxyapatite nanocomposites. *Carbohydr. Polym.* **2013**, *92*, 269−275.
(44) Dhillon, A.; Soni, S. K.; Kumar, D. Enhanced F^- removal performance by Ce−Zn binary metal oxide adsorption characteristics and mechanism. *J. Fluorine Chem.* **2017**, *199*, 67−76.
(45) Dhillon, A.; Kumar, D. Development of a nanoporous adsorbent for the removal of health-hazardous F^- ions from aqueous systems. *J. Mater. Chem. A* **2015**, *3*, 4215−4228.
(46) Zendehdel, M.; Shoshtari-Yeganeh, B.; Khanmohamadi, H.; Cruciani, G. Removal of fluoride from aqueous solution by adsorption on NaP: HAp Nanocomposite using response surface methodology. *Process Saf. Environ. Prot.* **2017**, *109*, 172−191.
(47) Prabhu, S. M.; Meenakshi, S. Synthesis of surface coated hydroxyapatite powders for F^- removal from aqueous solution. *Powder Technol.* **2014**, *268*, 306−315.
(48) Raghav, S.; Kumar, D. Adsorption equilibrium, kinetics, and thermodynamic studies of fluoride absorbed by tetrametallic oxide adsorbent. *J. Chem. Eng. Data* **2018**, *63*, 1682−1697.
(49) Kumar, M.; Tamilarasan, R. Kinetics and equilibrium studies on the removal of victoria blue using *Prosopis juliflora*-modified Carbon/Zn/Alginate polymer composite beads. *J. Chem. Eng. Data* **2013**, *58*, 517−527.
(50) Ahmad, M. A.; Alrozi, R. Removal of malachite green dye from aqueous solution using rambutan peel-based activated carbon: Equilibrium, kinetic and thermodynamic studies. *Chem. Eng. J.* **2011**, *171*, 510−516.
(51) Tan, I. A. W.; Ahmad, A. L.; Hameed, B. H. Adsorption isotherms, kinetics, thermodynamics and desorption studies of 2,4,6-trichlorophenol on oil palm empty fruit bunch-based activated carbon. *J. Hazard. Mater.* **2009**, *164*, 473−482.
(52) Rahman, N.; Haseen, U. Equilibrium modeling, kinetic, and thermodynamic studies on adsorption of Pb(II) by a hybrid inorganic−organic material: polyacrylamide zirconium(IV) iodate. *Ind. Eng. Chem. Res.* **2014**, *53*, 8198−8207.
(53) Sundaram, C. S.; Viswanathan, N.; Meenakshi, S. Defluoridation chemistry of synthetic hydroxyapatite at nano scale: Equilibrium and kinetic studies. *J. Hazard. Mater.* **2008**, *155*, 206−215.
(54) Dey, S.; Goswami, S.; Ghosh, U. C. Hydrous ferric oxide (HFO)—a scavenger for F^- from contaminated water. *Water Air Soil Pollut.* **2004**, *158*, 311−323.
(55) Velazquez-Jimenez, L. H.; Hurt, R. H.; Matos, J.; Rangel-Mendez, J. R. Zirconium carbon hybrid sorbent for F^- removal from water: oxalic acid mediated Zr(IV) assembly and adsorption mechanism. *Environ. Sci. Technol.* **2014**, *48*, 1166−1174.
(56) Ku, Y.; Chiou, H. M. The adsorption of F^- ion from aqueous solution by activated alumina. *Water, Air, Soil Pollut.* **2002**, *133*, 349−361.
(57) Tovar-Gómez, R.; Moreno-Virgen, M. R.; Dena-Aguilar, J. A.; Hernández-Montoya, V.; Bonilla-Petriciolet, A.; Montes-Morán, M. A. Modeling of fixed bed adsorption of fluoride on bone char using a

DOI: 10.1021/acsomega.8b01330
ACS Omega 2018, 3, 9675−9688

hybrid neural network approach. *Chem. Eng. J.* **2013**, *228*, 1098−1109.
(58) Atasoy, A. D.; Sahin, M. O. Adsorption of fluoride on raw and modified cement clay. *Clean: Soil Air Water.* **2014**, *42*, 415−420.

DOI: 10.1021/acsomega.8b01330
ACS Omega 2018, 3, 9675−9688